ResearchGate

See discussions, stats, and author profiles for this publication at: https://www.researchgate.net/publication/331769619

Micro-scale investigation of unsaturated sand in mini-triaxial shearing using X-ray CT

Article *in* Géotechnique Letters · March 2019

DOI: 10.1680/jgele.18.00214

CITATIONS
0

READS
368

5 authors, including:

Ji-Peng Wang
Shandong University
17 PUBLICATIONS **64** CITATIONS
SEE PROFILE

Edward Andò
French National Centre for Scientific Research
106 PUBLICATIONS **954** CITATIONS
SEE PROFILE

Simon Salager
Grenoble Institute of Technology
37 PUBLICATIONS **380** CITATIONS
SEE PROFILE

Pierre Lambert
Université Libre de Bruxelles
103 PUBLICATIONS **653** CITATIONS
SEE PROFILE

Some of the authors of this publication are also working on these related projects:

Wetting Dynamics - Experiments View project

Hydraulic Fracturing View project

All content following this page was uploaded by Ji-Peng Wang on 21 May 2019.

The user has requested enhancement of the downloaded file.

Wang, J.-P. *et al*. (2019) ***Géotechnique Letters*** **9**, 1–9, https://doi.org/10.1680/jgele.18.00214

Micro-scale investigation of unsaturated sand in mini-triaxial shearing using X-ray CT

J.-P. WANG*, E. ANDÒ†, P. CHARRIER†, S. SALAGER†, P. LAMBERT‡ and B. FRANÇOIS§

This paper explores the micro characteristics of unsaturated sand in triaxial shearing by using X-ray computed tomography (X-ray CT). To obtain higher resolution, a mini-triaxial set-up is designed in which the sample is miniaturised to 1 cm in diameter and 2 cm long, allowing scans with a pixel size of 9 μm. Samples are sheared in the mini-triaxial set-up at different constant suction levels (therefore, different degree of saturation). In the meanwhile, the samples are scanned by X-ray CT at various deformation stages, about 0, 2, 5, 10 and 15% axial strain. The three-dimensional (3D) reconstructed image is trinarised based on a region growing technique, which gives access to the microstructure of the solid, liquid and air phases. Then, the 3D image is subdivided into representative volume elements, with length $\approx 3{\cdot}8D_{50}$, which gives local information of degree of saturation and porosity. It is observed that the sample dilates and water drains out during triaxial test under constant suction condition. The local study shows that the porosity increase and water desaturation are more significant in the middle part of the sample, especially for a higher suction value. This work allows the emphasis of the coupling between dilatancy on shearing (highlighted by the evolution of local porosity) and the evolution of the local degree of saturation in unsaturated granular materials.

KEYWORDS: partial saturation; particle-scale behaviour; sands

ICE Publishing: all rights reserved

INTRODUCTION

Soils on the surface of the earth above the water table are usually partially saturated as a mixture of solid, air and water. The mechanical behaviour is therefore highly related to water content and liquid-phase morphology in the pores (Scheel *et al*., 2008). In the context of global warming, severe dry period and/or extreme rainfalls become more frequent in some areas, which may cause geo-disasters such as soil shrinkage leading to infrastructure settlement or landslides and slope failures (Smethurst *et al*., 2012). Therefore, a better understanding of macro–micro mechanics of unsaturated soils is crucial. Besides traditional unsaturated soil mechanics based on continuum principles (Bishop & Blight, 1963; Alonso *et al*., 1990; Fredlund & Rahardjo, 1993; Lu & Likos, 2004), study of the micro-characteristics of unsaturated granular media attracts much attention in the last two decades by using numerical methods, such as discrete element modelling (Scholtès *et al*., 2009; Duriez *et al*., 2018; Wang *et al*., 2018). However, most numerical studies are based on idealised assumptions and the liquid-phase content and morphology are limited to certain basic conditions.

With the development of X-ray computed tomography, non-invasive investigations on geomaterials become popular in recent years. It has been applied to study the micro-characteristics of granular material deformation (Hall *et al*., 2010; Andò *et al*., 2012; Vlahinić *et al*., 2014). As for unsaturated granular material, the X-ray tomography is also used to study the water-retention behaviour and the effect of non-homogeneity water at the grain scale (Bruchon *et al*., 2013; Wildenschild & Sheppard, 2013; Khaddour *et al*., 2018). However, the grain-scale deformation of unsaturated granular media under external loading and its coupling effect with the water-phase distribution still need more effort.

In this study, a customised mini-triaxial test device was designed for unsaturated soils, which reduced the sample size and gives a possibility of better resolution in X-ray tomography. Fine sand is sheared in this device under different suctions. The sample is scanned by X-ray CT at different strain stages and the micro-characteristics, such as local porosity and local water distribution, are studied.

EXPERIMENTAL METHOD

The design of the customised mini-triaxial test device is presented in Fig. 1(a). It is made of X-ray transparent materials based on the same principle of conventional triaxial test devices but with a reduced size. The sample size is 10 mm in diameter and 20 mm long. A submersible force sensor is employed and inserted into the axial piston in the confining chamber to avoid the friction effect between piston and the chamber orifice in force measurement. The sample is prepared in a latex membrane with a cylindrical mould (10 mm in diameter). The filled sand is fine sand with grain diameter ranging from 0·1 to 0·3 mm. After the mould is filled up, the top cap is fixed on the top and sealed with the membrane by an O ring. Before removing the cylindrical mould, a vacuum pump is used to apply vacuum in the sample through the bottom channel (top channel is closed). This is to maintain the sample vertically when assembling different parts and this also improves the sample saturation afterwards. After assembling, 16 kPa cell pressure is applied by a pressure controller. Then the bottom channel is also

Manuscript received 2 December 2018; first decision 12 March 2019; accepted 14 March 2019.
*School of Civil Engineering, Shandong University, Jinan, China (Orcid:0000-0001-7082-8864).
†CNRS, Grenoble INP (Institute of Engineering), Université Grenoble Alpes, 3SR, Grenoble, France.
‡TIPs Department, Université Libre de Bruxelles, Brussels, Belgium.
§BATir Department, Université Libre de Bruxelles, Brussels, Belgium.

Offprint provided courtesy of www.icevirtuallibrary.com
Author copy for personal use, not for distribution

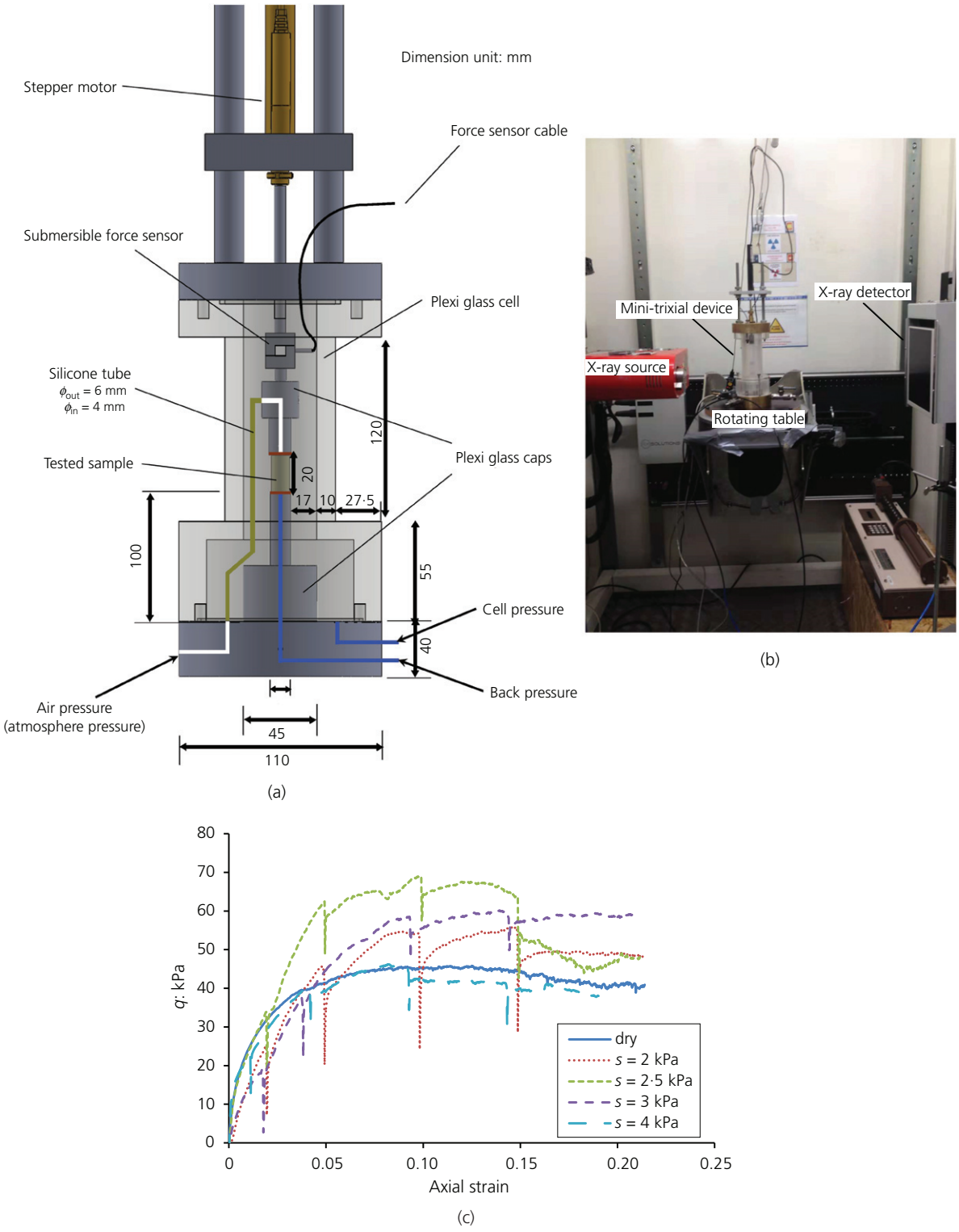

Fig. 1. Mini-triaxial shear test under X-ray scanning. (a) Mini-triaxial test device. (b) X-ray scan set-up. (c) Triaxial stress–strain behaviour

closed and connected to a water container. The bottom channel is then opened to allow water inflow to saturate the sample and the top channel is opened to the atmosphere. After water saturation, the water reservoir is lowered to a certain level to apply suctions (four tests with 2, 2·5, 3 and 4 kPa suctions are applied in this study). It takes about 20 min to reach the equilibrium state after applying suction. Evaporation and room humidity may not affect the test as there is no obvious change of water level in the reservoir during the test.

The triaxial cell is fixed on a rotational table in the micro-focus X-ray tomography chamber in Laboratoire 3SR, Grenoble (Fig. 1(b)) to conduct X-ray CT scans. Scans are performed at different strain stages (0, ≈2, ≈5, ≈10 and ≈15%) when the axial loading is ceased, keeping the axial piston at a fixed position. The loading rate is slow enough ($2{\cdot}5 \times 10^{-4}$ s^{-1}) to keep fully drained conditions. The deviatoric stress evolutions of the four triaxial tests are presented in Fig. 1(c). The behaviour of a dry sample is also presented as a reference. A slight decrease of the axial stress

Offprint provided courtesy of www.icevirtuallibrary.com
Author copy for personal use, not for distribution

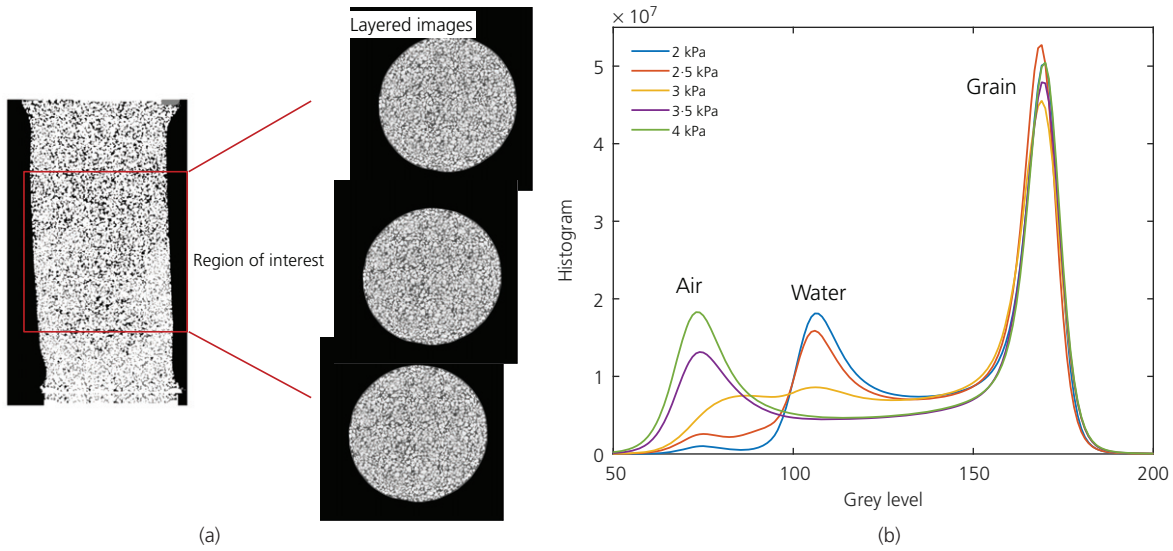

Fig. 2. Region of interest and histogram of the grey level

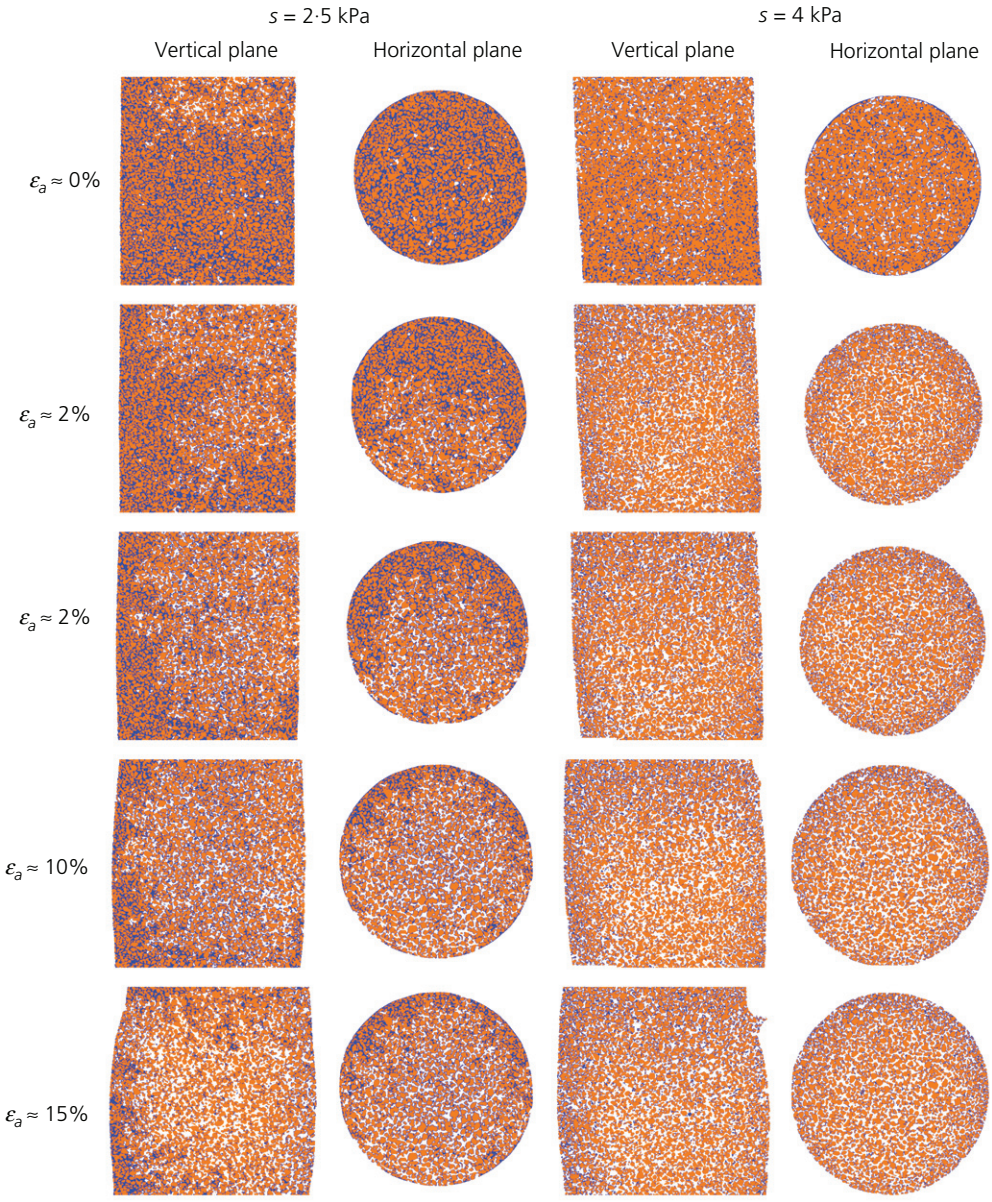

Fig. 3. Trinarised images of the triaxial tests with different suction (2·5 and 4 kPa) and at different strain levels

Offprint provided courtesy of www.icevirtuallibrary.com
Author copy for personal use, not for distribution

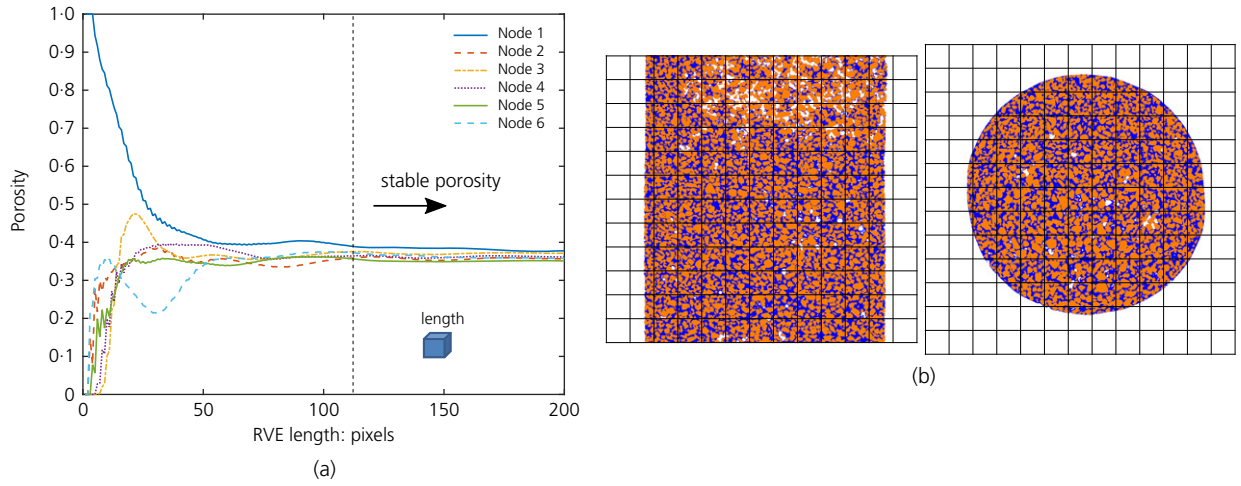

Fig. 4. (a) Determination of size of RVE. (b) Meshed image (RVE length = 110 pixels)

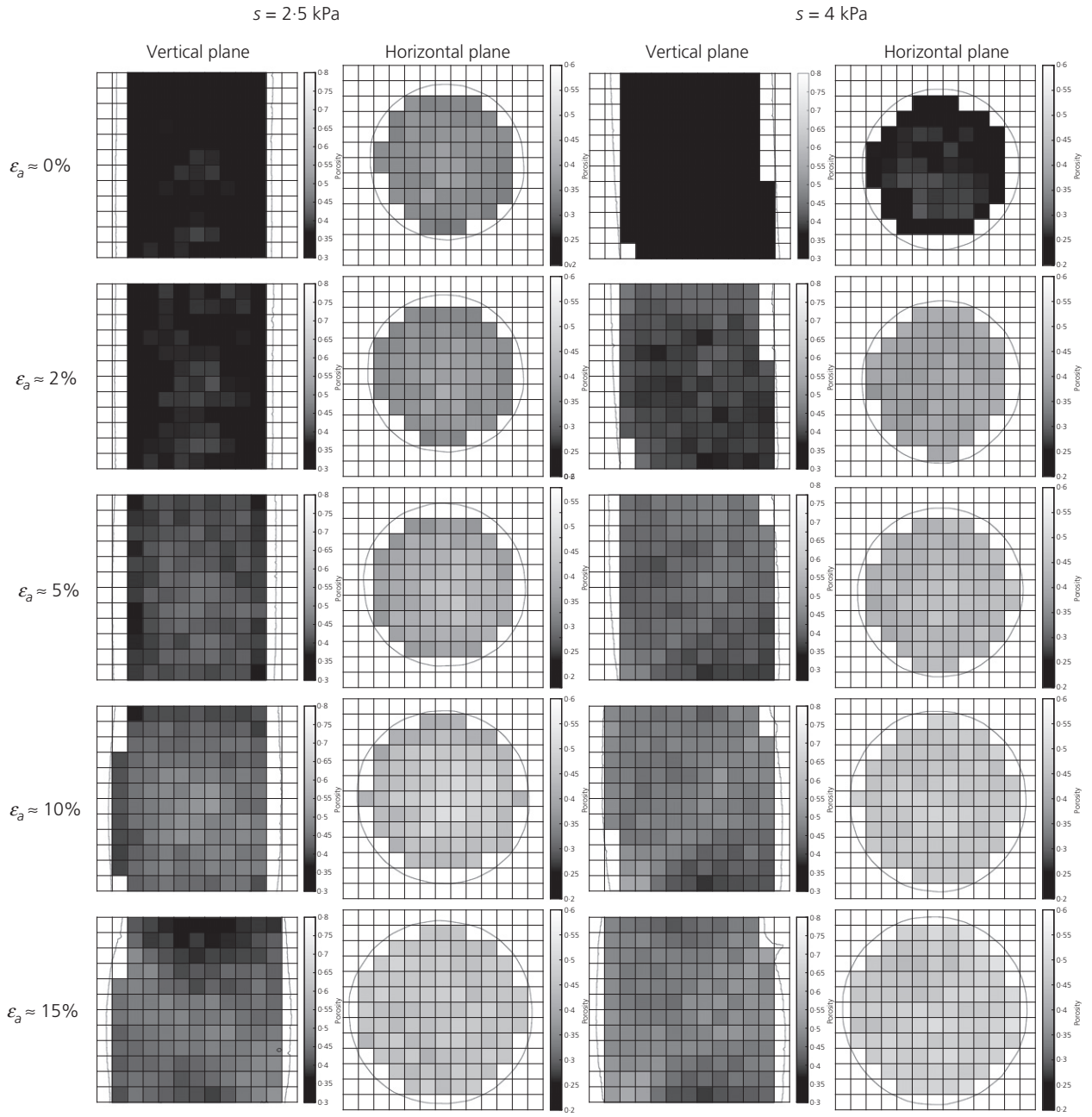

Fig. 5. Map of porosity of the triaxial tests at different strain levels

Offprint provided courtesy of www.icevirtuallibrary.com
Author copy for personal use, not for distribution

can be observed during the cease of the loading (on constant axial strain) due to relaxation processes but the whole stress–strain behaviour is not obviously affected by the pause of loading, as already observed in previous studies (Higo *et al.*, 2011). It can be seen that generally the unsaturated samples have higher material strength with a maximum strength for a suction of 2·5 kPa. Due to the relatively coarse particle size, the suction range of the sample is relatively low and the maximum strength is determined by the effective stress, which is a combination effect of suction and degree of saturation (Lu *et al.*, 2010; Wang *et al.*, 2017). For the specimens subjected to suctions of 3 and 4 kPa, the quantity of water stored in the meniscus after desaturation is not strong enough to produce a significant strength enhancement.

IMAGE TRINARISATION

To have a high image resolution in the X-ray scan, it requires either a small focused area or a large number of scanned positions (therefore longer scanning time). Since strain localisation mainly occurs in the middle part (Higo *et al.*, 2011), a region of interest (Fig. 2(a)) in the middle of the sample with 1·2 cm long is taken to perform the X-ray CT scan (2 h per scan). Finally, the obtained image resolution is 9 μm/pixel, which is close to the best resolution of this machine.

The series of X-ray projections were converted into a three-dimensional (3D) image (in the form of layered two-dimensional images) through the reconstruction process. Each pixel has a particular grey level, which is associated with its representing material – that is, solid,

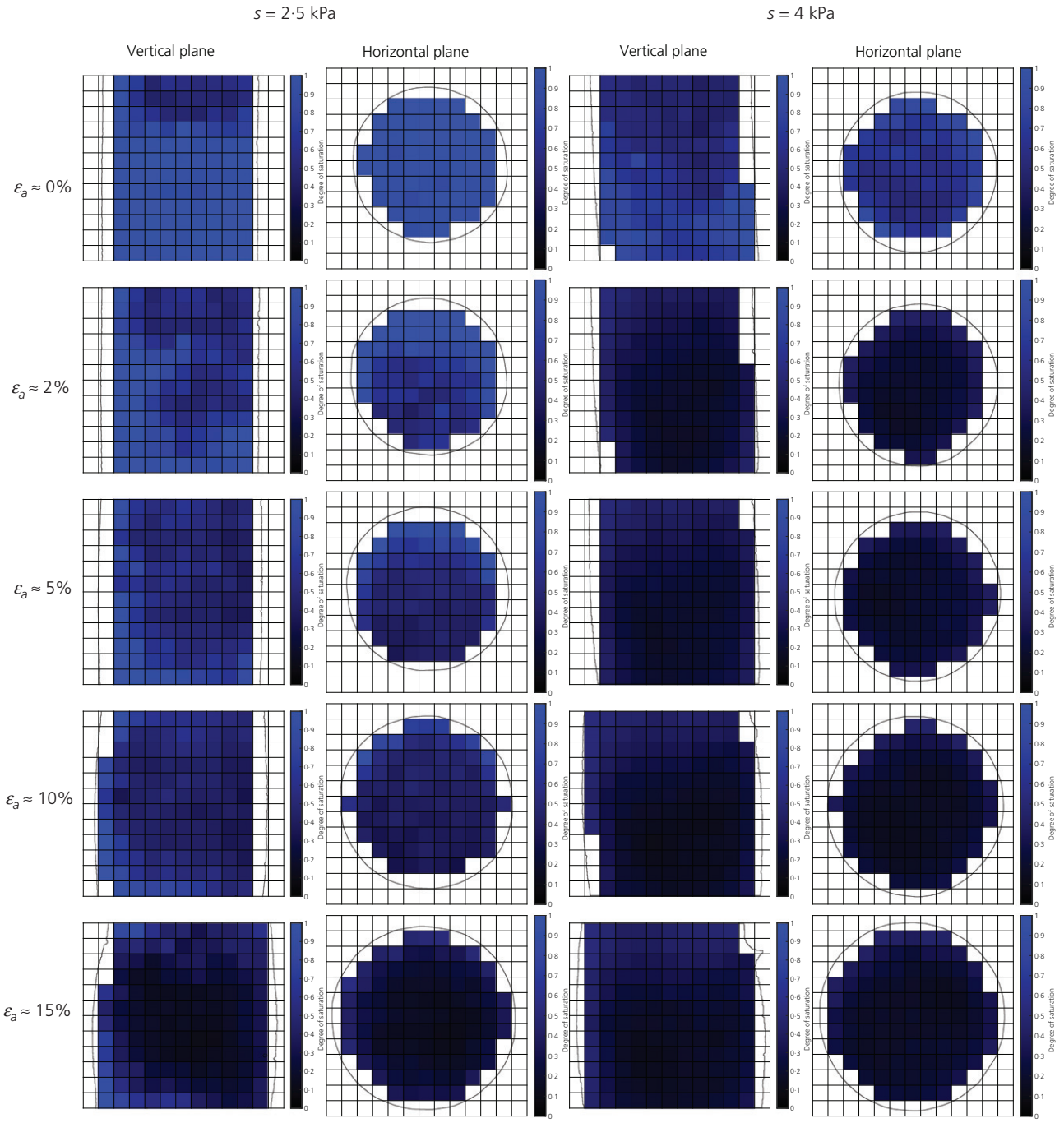

Fig. 6. Map of degree of saturation of the triaxial tests at different strain levels

Offprint provided courtesy of www.icevirtuallibrary.com
Author copy for personal use, not for distribution

water and air. Figure 2(b) shows the grey-level distributions of the initial samples with different suctions. The three peaks are air, water and grain, respectively. The authors used a segmentation technique adapted for three phases materials (Hashemi *et al*., 2013) to separate the different phases. It should be noted that at a low degree of saturation (for the higher suction), the quantity of water is not enough to exhibit a clear peak in the grey-level histogram. For this case, the authors used the same parameters of segmentation (in terms of grey levels) of the lower suction case, as the CT settings were the same.

Figure 3 illustrates the trinarised images of the triaxial tests with suction values of 2·5 and 4 kPa, respectively. Both the central vertical and central horizontal cross-sections are presented. It can be seen clearly that with the increase of axial strain, the sample is expanded horizontally. The pore water is not uniformly distributed on loading. As the specimen is dilated, the water is redistributed with the pore structure change. This is consistent with the observation in literature (Li *et al*., 2018) that highlight a lower probability of liquid cluster occurrence in larger pores. Moreover, there are some thin water layers on particle surface beyond the meniscus even though the partial volume effect is minimised. These could be some water droplets on the particles (Lourenço *et al*., 2012).

REPRESENTATIVE VOLUME ELEMENT-BASED ANALYSIS

The representative volume element (RVE) method (Khaddour *et al*., 2018; Wang *et al*., 2019) to quantify the local parameters of porosity and degree of saturation by meshing samples into cubic RVEs was used. The size of the RVE should be small enough but keeps the reliable information of the solid structure. To choose the RVE size, six RVEs are set on six nodes at different locations in the sample. The initial size of the RVEs is 1 pixel. In this case, the porosity of one RVE is either 0 (on the grain) or 1 (on air or water phase). With the increase of RVE length, the porosity values of the RVEs stabilise and become constants. After 110 pixels, the porosity value is almost constant (Fig. 4(a)). Therefore, the length of 110 pixels (≈1 mm) is taken as the RVE length and the sample is meshed into cubic elements (e.g. Fig. 4(b)). According to the size of the region of interest, the sample is divided into 12 layers of elements in the vertical direction.

Figure 5 depicts the porosity map of two representative triaxial tests (with 2·5 and 4 kPa suctions) in central vertical and horizontal planes based on the RVEs. It should be noted that there are some RVEs locating on the boundary of the sample and these elements are not included in the analysis. It can be seen that with triaxial strain, the strain localisation is developed as the porosity of the RVEs at the corresponding positions is increased (the colour becomes lighter). Figure 6 shows the map of the local degree of saturation of the two tests. At 0% strain, the sample with a lower suction has a higher degree of saturation throughout the sample. Although suction is maintained during the test, water content in the triaxial samples decreases on triaxial loading. The specimen with a higher suction desaturates more quickly.

Figure 7 demonstrates the relationship between local porosity and local degree of saturation based on the discrete

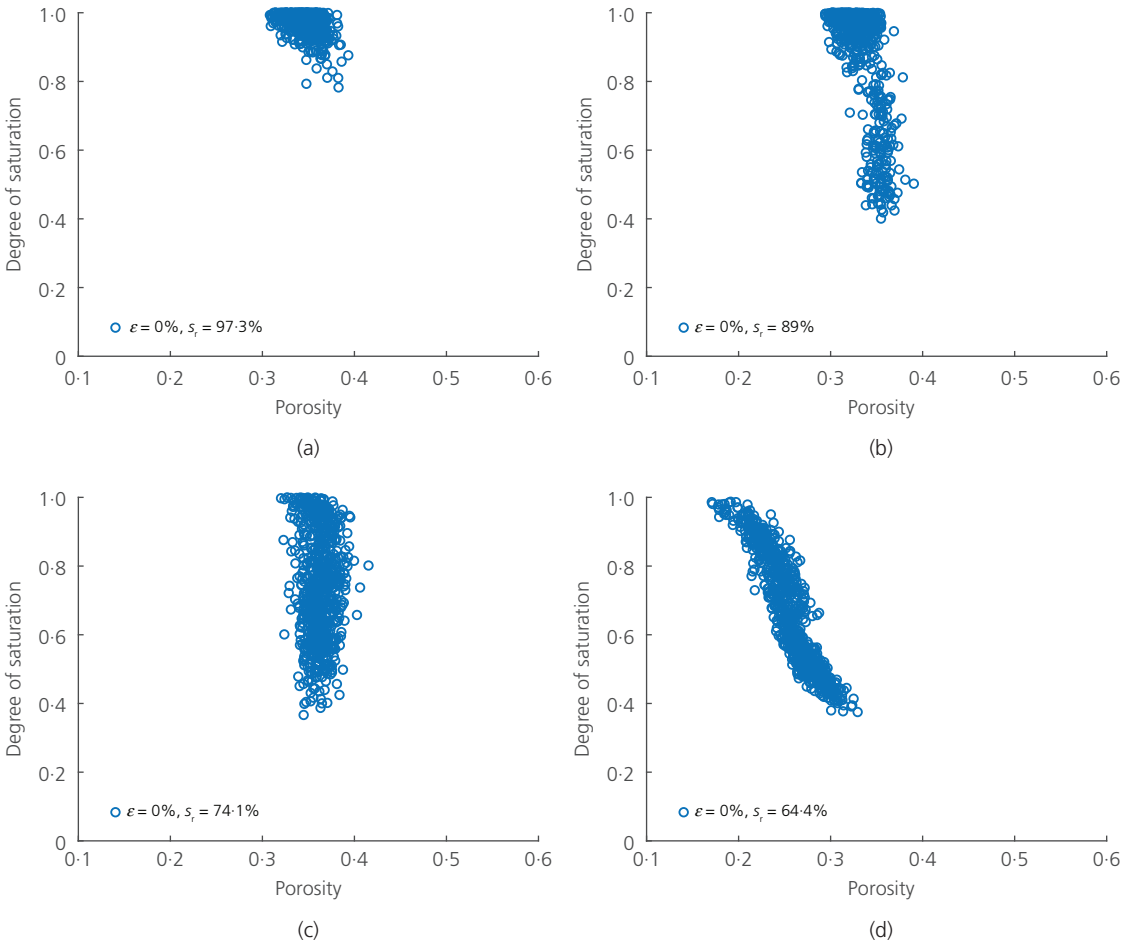

Fig. 7. RVE-based relationship between porosity and degree of saturation at the initial state. (a) Suction = 2 kPa; (b) suction = 2·5 kPa; (c) suction = 3 kPa; (d) suction = 4 kPa

Offprint provided courtesy of www.icevirtuallibrary.com
Author copy for personal use, not for distribution

RVEs for the initial states of the four tests before shearing. The overall degree of saturation of the scanned region is also presented in the caption. It is observed that the porosity is relatively homogeneous through the scanned zones, around 0·35, except for the specimen submitted to 4 kPa of suction for which the porosity varies from 0·15 to 0·35 (Fig. 7(d)). At this point it should be noted that the sample of 4 kPa suction with 0% strain was the first trial scan and the scan was conducted all over the sample. The image quality is lower than others. The results are presented anyway for further discussions.

Then, during triaxial shearing, the evolution of the local porosity and degree of saturation relationship is presented in Fig. 8. Loading induced deformation leads to porosity increase (due to dilatancy on shearing) and water desaturation in most elements. Consequently, after shearing, the elements with higher porosity have more chance to have a lower degree of saturation.

Figure 4 shows samples that are divided into 12 layers by the RVEs. The degree of saturation and porosity values in each layer can also be obtained. Figure 9 shows the degree of saturation and porosity in each layer in triaxial tests, in which the vertical axis is the layer number from bottom to the top. Initially, the porosity is uniformly distributed through all the samples around a value of 0·35, except for the specimen submitted to 4 kPa of suction, which is due to the deficiency in image quality of the first scan of this sample and the possibly induced larger porosity measurement error. It also indicates that a small change in microstructure by axial strain may lead to a significant desaturation under a constant suction. At the end of the shearing (at 15% of axial deformation), the porosity is larger for higher suction. In other words, it means that the specimen exhibits higher dilatancy on shearing at higher suction. This is consistent with usual unsaturated soil mechanics. Suction induces an over-consolidation effect that, in turn, generated dilatancy on shearing. Also, it can be seen that during triaxial compression, the porosity increase is remarkably higher in the middle part of the specimen. Consequently, the drop of degree of saturation is larger in the central layers.

CONCLUSIONS

A miniaturised suction-controlled triaxial test device was developed for micro-CT investigation. Fine sand was sheared in the set-up under different suctions with scans conducted at different strain stages and a resolution of 9 μm/pixel was achieved. The reconstructed images were then trinarised in the three-dimensional space by a region growing method. The samples were meshed into cubic RVEs to study local information. The RVE length was chosen as 3·8 times of the mean grain size (110 pixels). Local porosity and local degree of saturation were therefore obtained based on the RVEs.

From the RVE mapping on porosity and degree of saturation, it demonstrates the strain concentration in the central part of the specimen. Under constant suction, the samples desaturated due to soil dilation (porosity increase) on triaxial loading. Statistically, a higher porosity after shearing means a lower degree of saturation in the RVEs.

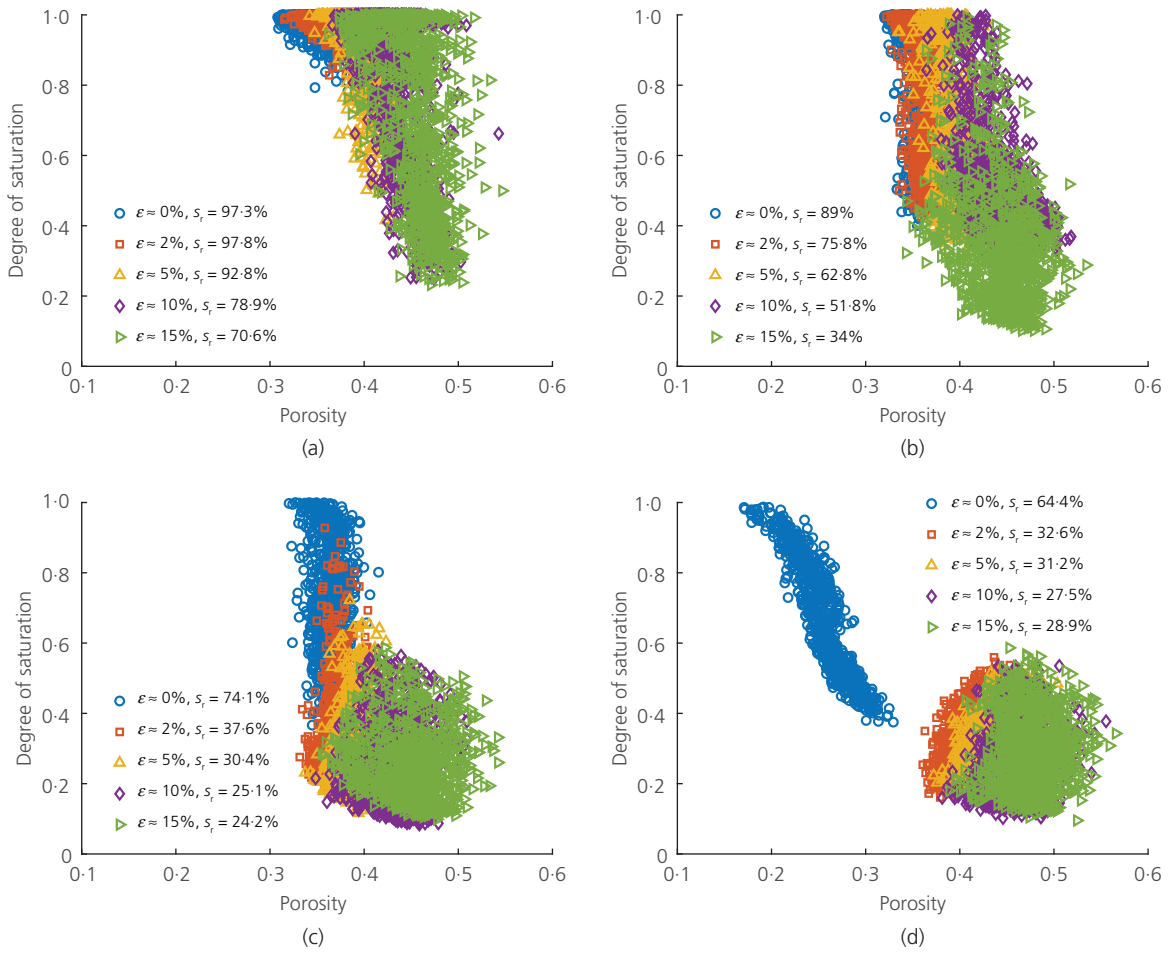

Fig. 8. RVE-based relationship between porosity and degree of saturation at different strain stages. (a) Suction = 2 kPa; (b) suction = 2·5 kPa; (c) suction = 3 kPa; (d) suction = 4 kPa

Offprint provided courtesy of www.icevirtuallibrary.com
Author copy for personal use, not for distribution

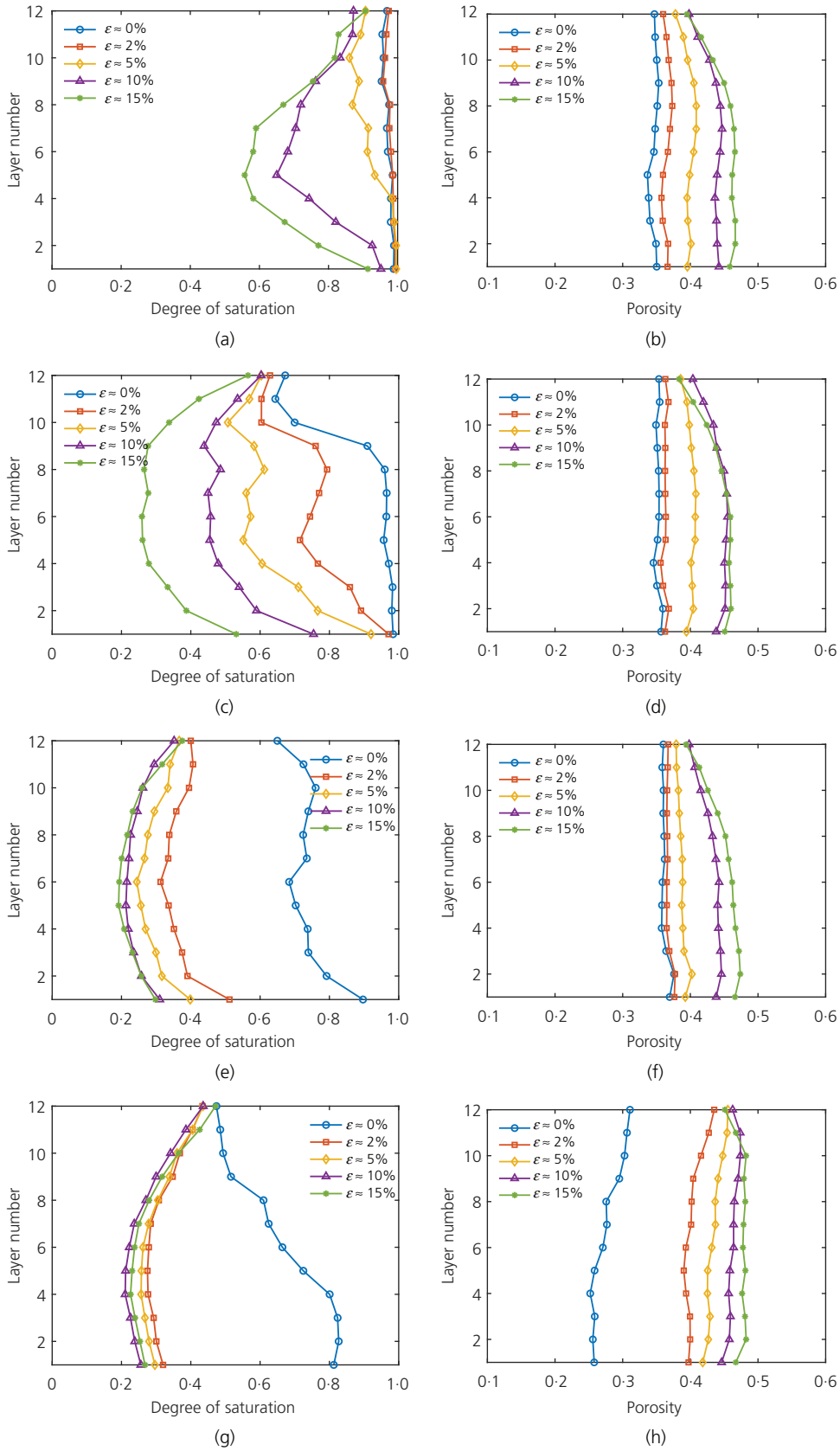

Fig. 9. Degree of saturation and porosity in different layers of the four samples. (a) Suction = 2 kPa, saturation; (b) suction = 2 kPa, porosity; (c) suction = 2·5 kPa, saturation; (d) suction = 2·5 kPa, porosity; (e) suction = 3 kPa, saturation; (f) suction = 3 kPa, porosity; (g) suction = 4 kPa, saturation; (h) suction = 4 kPa, porosity

A layered study also shows that the middle part of the sample has a higher porosity and lower degree of saturation than those of the two ends after triaxial shearing. These mean that it may not be suitable to directly use the initial state water-retention property to predict the failure and critical state behaviours. The coupled local deformation and water

Offprint provided courtesy of www.icevirtuallibrary.com
Author copy for personal use, not for distribution

redistribution/inhomogeneity effect should be considered, especially for a continuous deformation condition, such as triaxial test.

This local analysis of the link between porosity and degree of saturation on triaxial shearing is based on the sub-division of the scanned zone into cubic RVEs. In this approach, the local behaviour is evaluated in terms of volumetric response. Further investigations are currently performed to deduce local strain components through a discrete particle tracking approach and Delaunay triangulation in order to evaluate the local dilatancy response (link between deviatoric and volumetric strains) together with local saturation degree evolution.

ACKNOWLEDGEMENT

This work was funded by F.R.S-FNRS of Belgium with project number: PDR.T.1002·14. The first author also appreciates the support of Taishan Scholar Project of Shandong Province of China during paper writing and revision.

REFERENCES

Alonso, E. E., Gens, A. & Josa, A. (1990). A constitutive model for partially saturated soils. *Géotechnique* **40**, No. 3, 405–430, https://doi.org/10.1680/geot.1990.40.3.405.

Andò, E., Hall, S. A., Viggiani, G., Desrues, J. & Bésuelle, P. (2012). Grain-scale experimental investigation of localised deformation in sand: a discrete particle tracking approach. *Acta Geotech.* **7**, No. 1, 1–13, https://doi.org/10.1007/s11440-011-0151-6.

Bishop, A. W. & Blight, G. E. (1963). Some aspects of effective stress in saturated and partly saturated soils. *Géotechnique* **13**, No. 3, 177–197, https://doi.org/10.1680/geot.1963.13.3.177.

Bruchon, J. F., Pereira, J. M., Vandamme, M., Lenoir, N., Delage, P., Bornert, M., Bruchon, J. F., Pereira, J. M., Vandamme, M., Lenoir, N., Delage, P. & Bornert, M. (2013). Full 3D investigation and characterisation of capillary collapse of a loose unsaturated sand using X-ray CT. *Gran. Matter* **15**, No. 6, 783–800, https://doi.org/10.1007/s10035-013-0452-6.

Duriez, J., Wan, R., Pouragha, M. & Darve, F. (2018). Revisiting the existence of an effective stress for wet granular soils with micromechanics. *Int. J. Numer. Anal. Methods Geomech.* **42**, No. 8, 959–978, https://doi.org/10.1002/nag.2774.

Fredlund, D. G. & Rahardjo, H. (1993). *Soil mechanics for unsaturated soils*. John Wiley & Sons, New York, USA.

Hall, S. A., Bornert, M., Desrues, J., Pannier, Y., Lenoir, N., Viggiani, G. & Bésuelle, P. (2010). Discrete and continuum analysis of localised deformation in sand using X-ray μCT and volumetric digital image correlation. *Géotechnique* **60**, No. 5, 315–322, https://doi.org/10.1680/geot.2010.60.5.315.

Hashemi, M. A., Khaddour, G., François, B., Massart, T. J. & Salager, S. (2013). A tomographic imagery segmentation methodology for three-phase geomaterials based on simultaneous region growing. *Acta Geotech.* **9**, No. 5, 831–846, https://doi.org/10.1007/s11440-013-0289-5.

Higo, Y., Oka, F., Kimoto, S., Sanagawa, T. & Matsushima, Y. (2011). Study of strain localization and microstructural changes in partially saturated sand during triaxial tests using microfocus X-ray CT. *Soils Found.* **51**, No. 1, 95–111, https://doi.org/10.3208/sandf.51.95.

Khaddour, G., Riedel, I., Andò, E., Charrier, P., Bésuelle, P., Desrues, J., Viggiani, G. & Salager, S. (2018). Grain-scale characterization of water retention behaviour of sand using X-ray CT. *Acta Geotech.* **13**, No. 3, 497–512, https://doi.org/10.1007/s11440-018-0628-7.

Li, S., Liu, M., Hanaor, D. & Gan, Y. (2018). Dynamics of viscous entrapped saturated zones in partially wetted porous media. *Transport Porous Media* **125**, No. 2, 193–210, https://doi.org/10.1007/s11242-018-1113-3.

Lourenço, S. D. N., Gallipoli, D., Augarde, C. E., Toll, D. G., Fisher, P. C. & Congreve, A. (2012). Formation and evolution of water menisci in unsaturated granular media. *Géotechnique* **62**, No. 3, 193–199, https://doi.org/10.1680/geot.11.P.034.

Lu, N. & Likos, W. J. (2004). *Unsaturated soil mechanics*. John Wiley, Hoboken, NJ, USA.

Lu, N., Godt, J. W. & Wu, D. T. (2010). A closed-form equation for effective stress in unsaturated soil. *Water Resour. Res.* **46**, No. 5, W05515, https://doi.org/10.1029/2009WR008646.

Scheel, M., Seemann, R., Brinkmann, M., Di Michiel, M., Sheppard, A., Breidenbach, B. & Herminghaus, S. (2008). Morphological clues to wet granular pile stability. *Nat. Mater.* **7**, No. 3, 189–193, https://doi.org/10.1038/nmat2117.

Scholtès, L., Hicher, P., Nicot, F., Chareyre, B. & Darve, F. (2009). On the capillary stress tensor in wet granular materials. *Int. J. Numer. Anal. Methods Geomech.* **33**, No. 10, 1289–1313, https://doi.org/10.1002/nag.767.

Smethurst, J., Clarke, D. & Powrie, W. (2012). Factors controlling the seasonal variation in soil water content and pore water pressures within a lightly vegetated clay slope. *Géotechnique* **62**, No. 5, 429–446, https://doi.org/10.1680/geot.10.P.097.

Vlahinić, I., Andò, E., Viggiani, G. & Andrade, J. (2014). Towards a more accurate characterization of granular media: extracting quantitative descriptors from tomographic images. *Gran. Matter* **16**, No. 1, 9–21, https://doi.org/10.1007/s10035-013-0460-6.

Wang, J. P., Hu, N., François, B. & Lambert, P. (2017). Estimating water retention curves and strength properties of unsaturated sandy soils from basic soil gradation parameters. *Water Resour. Res.* **53**, No. 7, 6069–6088, https://doi.org/10.1002/2017WR020411.

Wang, J. P., Li, X. & Yu, H. S. (2018). A micro–macro investigation of the capillary strengthening effect in wet granular materials. *Acta Geotech.* **13**, No. 3, 513–533, https://doi.org/10.1007/s11440-017-0619-0.

Wang, J. P., Lambert, P., DeKock, T., Cnudde, V. & François, B. (2019). Investigation of the effect of specific interfacial area on strength of unsaturated granular materials by X-ray tomography image analysis. *Acta Geotech.*, https://doi.org/10.1007/s11440-019-00765-2).

Wildenschild, D. & Sheppard, A. P. (2013). X-ray imaging and analysis techniques for quantifying pore-scale structure and processes in subsurface porous medium systems. *Adv. Water Resour.* **51**, 217–246, https://doi.org/10.1016/j.advwatres.2012.07.018.

HOW CAN YOU CONTRIBUTE?

To discuss this paper, please submit up to 500 words to the editor at journals@ice.org.uk. Your contribution will be forwarded to the author(s) for a reply and, if considered appropriate by the editorial board, it will be published as a discussion in a future issue of the journal.

Offprint provided courtesy of www.icevirtuallibrary.com
Author copy for personal use, not for distribution

View publication stats